

Real-time hybrid simulation of a multi-story wood shear wall with first-story experimental substructure incorporating a rate-dependent seismic energy dissipation device

Xiaoyun Shao^{*1}, John van de Lindt², Pouria Bahmani², Weichiang Pang³, Ershad Ziaei³, Michael Symans⁴, Jingjing Tian⁴ and Thang Dao⁵

¹Department of Civil and Construction Engineering, Western Michigan University, Kalamazoo, MI, USA

²Department of Civil and Environmental Engineering, Colorado State University, Fort Collins, CO, USA

³Glenn Department of Civil and Environmental Engineering, Clemson University, Clemson, SC, USA

⁴Department of Civil and Environmental Engineering, Rensselaer Polytechnic Institute Troy, NY, USA

⁵Department of Civil, Construction and Environmental Engineering, The University of Alabama, Tuscaloosa, AL, USA

(Received May 20, 2014, Revised August 15, 2014, Accepted August 20, 2014)

Abstract. Real-time hybrid simulation (RTHS) of a stacked wood shear wall retrofitted with a rate-dependent seismic energy dissipation device (viscous damper) was conducted at the newly constructed Structural Engineering Laboratory at the University of Alabama. This paper describes the implementation process of the RTHS focusing on the controller scheme development. An incremental approach was adopted starting from a controller for the conventional slow pseudodynamic hybrid simulation and evolving to the one applicable for RTHS. Both benchmark- scale and full-scale tests are discussed to provide a roadmap for future RTHS implementation at different laboratories and/or on different structural systems. The developed RTHS controller was applied to study the effect of a rate-dependent energy dissipation device on the seismic performance of a multi-story wood shear wall system. The test specimen, setup, program and results are presented with emphasis given to inter-story drift response. At 100% DBE the RTHS showed that the multi-story shear wall with the damper had 32% less inter-story drift and was noticeably less damaged than its un-damped specimen counterpart.

Keywords: real-time hybrid simulation; wood shear wall; energy dissipation; viscous damper; time delay compensation

1. Introduction

Real-time hybrid simulation (RTHS) has seen increased attention over the past decade due to the similarity of its test setup relative to that of conventional pseudodynamic testing, applicability to study structural systems with rate-dependent behavior, and its capability of providing an economical and efficient method for experimental testing as compared to shake table testing. During an RTHS, a structural system under investigation is divided into two or more

*Corresponding author, Associate Professor, E-mail: xiaoyun.shao@wmich.edu

complementary parts. The part being physically tested using hydraulic loading equipment is an *experimental substructure* and the remaining part being numerically simulated is referred to as a *numerical substructure*. Real-time calculation of the target displacement is conducted and its value is transferred through a real-time controller to the hydraulic actuator that is used to impose the target displacement to the experimental substructure. Meanwhile, the restoring force measured from the experimental substructure is fed back to the numerical simulation to determine the target displacement for the next step. Thus a *closed-loop experiment* is formed that integrates numerical and physical components into one structural response simulation. Essentially RTHS is rooted in the conventional slow pseudodynamic (PSD) testing but is conducted in real-time and employing substructure partitioning and integration.

RTHS was first introduced by Nakashima *et al.* (1992) to test a structure with viscous damper. Since then the development of this experimental method has focused on time delay compensation of the actuators and fast integration algorithms to ensure stable execution and reliable numerical simulation results (Horiuchi *et al.* 1996, Darby *et al.* 1999, Shing *et al.* 2006, Carrion and Spencer 2008, Ahmadizadeh and Mosqueda 2008). RTHS has primarily been applied to seismic evaluations of structures installed with devices that have nonlinear and rate-dependent behavior, such as steel frame structures with MR dampers (Chae *et al.* 2013, Phillips and Spencer 2013) and steel frame structures with nonlinear viscous dampers and elastomeric dampers (Mercan and Ricles 2009). The dynamic performance of bridges equipped with friction-based seismic isolators (Dion *et al.* 2012) and viscous seismic protective devices (Dion *et al.* 2011) were also assessed using RTHS. More recently, RTHS of a non-ductile reinforced concrete frame was reported by Saouma *et al.* (2013).

Though RTHS and hybrid simulation are seeing increasing application in earthquake engineering projects, few experiments have been carried out on wood-frame structures. In a French-Japanese project, both static tests and PSD simulations were conducted on wood-framed shear walls with an opening and these experimental results were used to validate a finite-element code for its application to dynamic analysis of wood shear walls (Richard *et al.* 2003). A series of PSD tests on several plywood-sheathed conventional wooden shear walls were conducted in Japan (Yasumura and Yasui 2006, Yasumura *et al.* 2006, Kamada *et al.* 2011). The test results were compared to their respective numerical time-history analysis using a lumped-mass model and hysteresis model and reasonable agreement was obtained. Without exception, the PSD simulations conducted thus far on wood-frame structures were slow tests without numerical substructures (i.e., without numerical wood structural components).

This paper presents an RTHS of a three-story stacked wood shear wall retrofitted with a rate-dependent energy dissipation device (linear fluid viscous damper) which was conducted as part of the NEES-Soft project (a five-university collaborative project entitled "Seismic Risk Reduction for Soft-Story Woodframe Buildings"; van de Lindt *et al.* 2012). The experimental substructure was the first story wall, retrofitted with a viscous damper, while the walls in the upper two stories were numerically simulated. The implementation process of the RTHS including the numerical simulation and the controller scheme development is discussed in detail. Both benchmark-scale and full-scale testing were performed, providing a roadmap for future RTHS implementation involving multiple laboratories and/or different structural systems. The developed RTHS controller was applied to study the effect of the viscous damper on the seismic performance of the multi-story wood shear wall. The test specimen, setup, program and results are presented with emphasis given to the inter-story drift response as a measure of damage.

2. Numerical simulation and integration algorithm

The real-time hybrid simulation (RTHS) in this study required two major developments, namely numerical simulation and physical testing, which were carried out at Clemson University and Western Michigan University (WMU), respectively. Matlab/Simulink was used in both tasks, making the integration of these two tasks as seamless as possible. This section and the following section present the development of the numerical simulation and the RTHS controller in detail.

2.1 Numerical model for wood-frame building

A schematic view of the three-story stacked shear wall model is shown in Fig. 1. In this displacement-based RTHS, the upper stories were numerically modeled while the first story was physically represented with either (1) a conventional light-frame wood shear wall or (2) the same shear wall with a fluid viscous damper. The hybrid stacked shear wall system was modeled as a three degrees-of-freedom (3DOF) lumped mass system (Fig. 1(b)). All three seismic weights (masses) were defined numerically. Numerical modeling of the hysteretic response of conventional light-frame wood shear walls was the focus of many studies in the past (e.g., Stewart 1987, Dolan 1989, Folz and Filiatrault 2001, Pang *et al.* 2007). Due to its simplicity and low computational overhead when coded into a Matlab/Simulink program, the modified Stewart (MSTEW) hysteretic model, also known as the CUREE hysteretic model (Stewart 1987, Folz and Filiatrault 2001), was utilized to characterize the hysteretic behavior of the shear walls in the upper two stories. Fig. 2 depicts the modeling parameters of the MSTEW model. In addition to numerically modeling the masses and the upper story shear walls, the damping matrix was defined numerically using a Rayleigh damping formulation in which a damping ratio of 5% (of critical damping) was assigned to the first two modes of vibration. The numerical model, developed by Clemson University, was coded into a Simulink program and was used to compute the displacement response to be applied to the physical first story in RTHS. The solution of the equation of motion (EOM) was obtained via a modified implicit Newmark- β integration algorithm as discussed in Section 2.2.

The EOM of the three-story stacked shear wall can be expressed as

$$M\ddot{u} + C\dot{u} + f(u, \dot{u}) = p(\ddot{u}_g) \quad (1)$$

where M and C are the mass and damping matrices; \ddot{u} , \dot{u} and u are the acceleration, velocity and displacement vectors, respectively. $f(u, \dot{u})$ is the restoring force vector which depends on the magnitude and sign of the displacement and velocity and thus is history-dependent, $p(\ddot{u}_g)$ is the applied dynamic load which is a function of the ground acceleration, \ddot{u}_g .

In this RTHS, the three-story stacked shear wall system is modeled as a 3DOF lumped-mass system. The mass matrix is a diagonal matrix = $\text{diag}(m_1, m_2, m_3)$ where m_1 , m_2 and m_3 are the lumped numerical masses. Note that, in this formulation, only the horizontal translational DOFs are analyzed and P-delta effect is not considered. In Eq. (1), $p(\ddot{u}_g)$ is the applied earthquake force vector, which is a function of the ground acceleration \ddot{u}_g and the lumped masses

$$p(\ddot{u}_g) = -[m_1 \ m_2 \ m_3]^T \ddot{u}_g \quad (2)$$

The damping matrix is defined using the mass and stiffness proportional Rayleigh damping

$$C = a_o M + a_1 K \tag{3}$$

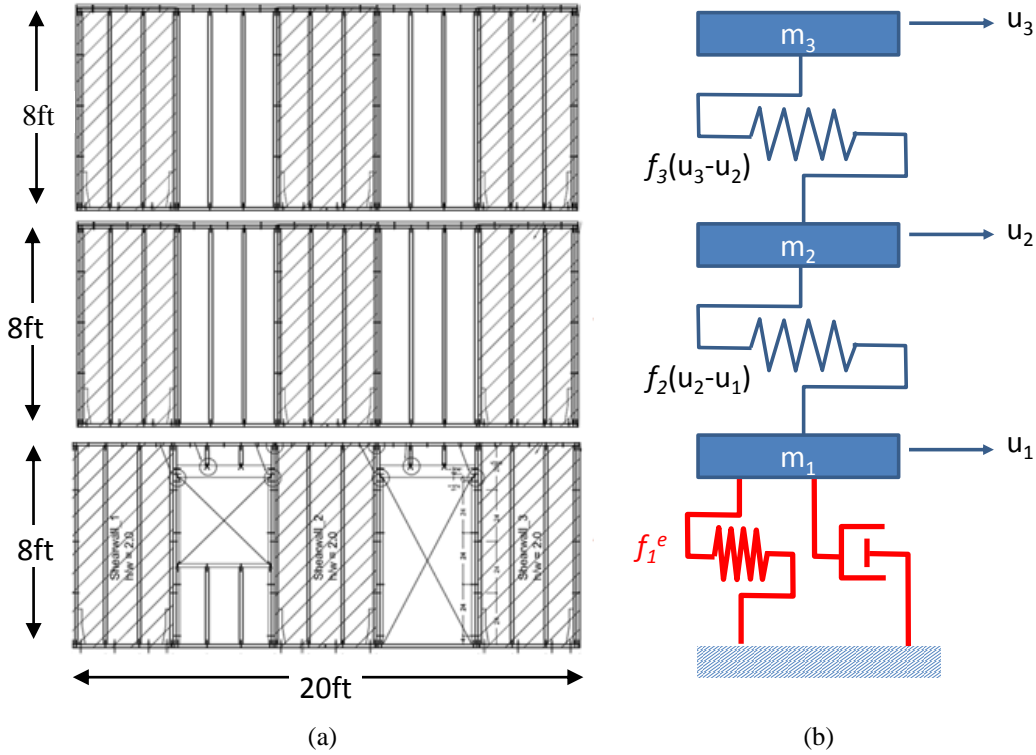


Fig. 1 Hybrid three-story stacked wood shear wall system with the first-story physically represented and the upper stories numerically simulated: (a) schematic view; and (b) depiction of numerical model (1ft = 0.305 m)

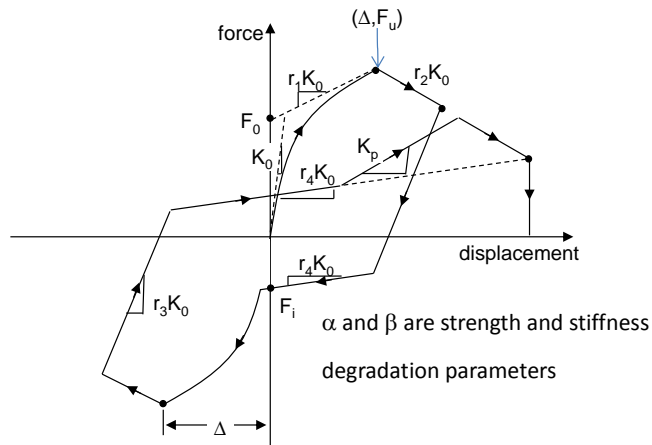


Fig. 2 Nonlinear hysteretic spring model for the shear walls in the upper two stories

where coefficients a_o and a_1 are computed as

$$a_o = \frac{2\omega_1\omega_2}{\omega_1 + \omega_2} \zeta \quad a_1 = \frac{2}{\omega_1 + \omega_2} \zeta \quad (4)$$

Here, ω_1 and ω_2 are the frequencies of modes 1 and 2. Eq. (4) assumes the same damping ratio for both the first and second modes ($\zeta = 0.05$ of critical damping).

2.2 Integration algorithm – Implicit Newmark- β

The implicit Newmark- β integration scheme with iterations is the most common integrator employed to solve the EOM (i.e., Eq. (1)) for pure numerical models. This is because the implicit Newmark- β integrator is unconditionally stable. However, the path-dependent nature of the physical first-story specimen does not permit the direct implementation of the implicit Newmark- β integration scheme in RTHS. Iterative displacements applied to experimental substructures will cause unrecoverable and unrealistic strength degradations and fatigue damage to the test specimen. For RTHS, explicit integration procedures are widely used since they do not require iteration and are simple to implement. While simple to implement, conventional explicit integration algorithms are only conditionally stable and typically require a very small integration time step in order to achieve numerical stability. With recent advancements in RTHS method, several unconditionally stable explicit integration algorithms, such as the CR integration (Chen *et al.* 2008), were developed.

In this RTHS, a modified implicit Newmark- β integrator that does not impose iterative displacements on the physical substructure was developed and used. The EOM (Eq. (1)) can be rewritten in terms of the tangent stiffness matrix and the incremental acceleration, velocity, displacement and earthquake force vectors

$$M \begin{Bmatrix} \Delta\ddot{u}_1 \\ \Delta\ddot{u}_2 \\ \Delta\ddot{u}_3 \end{Bmatrix} + C \begin{Bmatrix} \Delta\dot{u}_1 \\ \Delta\dot{u}_2 \\ \Delta\dot{u}_3 \end{Bmatrix} + \begin{bmatrix} k_1^e + k_2 & -k_2 & 0 \\ -k_2 & k_2 + k_3 & -k_3 \\ 0 & -k_3 & k_3 \end{bmatrix} \begin{Bmatrix} \Delta u_1 \\ \Delta u_2 \\ \Delta u_3 \end{Bmatrix} = \begin{Bmatrix} \Delta p_1 \\ \Delta p_2 \\ \Delta p_3 \end{Bmatrix} \quad (5)$$

where $\Delta\ddot{u}_i$, $\Delta\dot{u}_i$, Δu_i , Δp_i , and k_i are incremental acceleration, velocity, displacement, force and tangent stiffness of the i -th story, respectively. Note that superscript “ e ” in Eq. (5) and subsequent equations denotes terms that are associated with the experimental substructure and thus the values are determined experimentally during RTHS. Except for the k_1^e term, which is the initial tangent stiffness of the physical first-story specimen, all other terms in Eq. (5) are numerically modeled. Prior to the RTHS, the initial tangent stiffness of the physical substructure was determined via a low amplitude cyclic test. The values of k_2 and k_3 for each integration step were obtained from the numerical model (i.e., the MSTEW hysteretic model, see Table 5). Using the initial tangent stiffness of the experimental substructure to populate the tangent stiffness matrix, Eq. (5) was solved using the implicit Newmark- β method without iteration to obtain the incremental displacements for the *first integration step*:

$$\Delta \bar{p}^i = \Delta p^i + \left(\frac{M}{\beta \Delta t} + \frac{\gamma C}{\beta} \right) \dot{u}^i + \left(\frac{M}{2\beta} + \Delta t \left(\frac{\gamma}{2\beta} - 1 \right) C \right) \ddot{u}^i \quad (6)$$

$$\bar{K}^i = K^i + \frac{\gamma}{\beta \Delta t} C + \frac{1}{\beta \Delta t^2} M \quad (7)$$

$$\Delta \bar{p}^i = \bar{K}^i \Delta u^i \quad (8)$$

$$u^{i+1} = u^i + \Delta u^i \quad (9)$$

Here, $\Delta \bar{p}^i$ is the incremental effective force and \bar{K} is the effective dynamic tangent stiffness which includes the mass and damping terms; u and \ddot{u} are displacement and acceleration; γ and β are the Newmark- β integration constants, which are $\frac{1}{2}$ and $\frac{1}{4}$, respectively, for the constant average acceleration method. Δt is the integration time step and the superscript i indicates the time step number. Using the incremental displacements obtained from Eq. (8), the incremental velocities and accelerations were computed as follows

$$\Delta \dot{u}^i = \frac{\gamma}{\beta \Delta t} \Delta u^i - \frac{\gamma}{\beta} \dot{u}^i + \Delta t \left(1 - \frac{\gamma}{2\beta} \right) \ddot{u}^i \quad (10)$$

$$\Delta \ddot{u}^i = \frac{1}{\beta \Delta t^2} \Delta u^i - \frac{1}{\beta \Delta t} \dot{u}^i - \frac{1}{2\beta} \ddot{u}^i \quad (11)$$

The first-story displacement, obtained by solving Eqs. (6)-(9) was passed to the hybrid simulation controller to move the actuator to the target displacement. Once the actuator reached the first target displacement, the restoring force for the first story physical wall, f_1 , was measured and the increment was determined as follows

$$\Delta f_1^e = f_1^{i+1} - f_1^i \quad (12)$$

where f_1^{i+1} and f_1^i are the restoring forces of the current and previous integration steps. Note that the initial stiffness and Eq. (5) were only utilized once at the beginning of the test to start the integration process. For the subsequent integration steps, the tangent stiffness of the experimental substructure was removed from the tangent stiffness matrix and the incremental force of the physical first-story was added to the right-hand side of the equation

$$M \begin{Bmatrix} \Delta \ddot{u}_1 \\ \Delta \ddot{u}_2 \\ \Delta \ddot{u}_3 \end{Bmatrix} + C \begin{Bmatrix} \Delta \dot{u}_1 \\ \Delta \dot{u}_2 \\ \Delta \dot{u}_3 \end{Bmatrix} + \begin{bmatrix} k_2 & -k_2 & 0 \\ -k_2 & k_2 + k_3 & -k_3 \\ 0 & -k_3 & k_3 \end{bmatrix} \begin{Bmatrix} \Delta u_1 \\ \Delta u_2 \\ \Delta u_3 \end{Bmatrix} = \begin{Bmatrix} \Delta p_1 - \Delta f_1^e \\ \Delta p_2 \\ \Delta p_3 \end{Bmatrix} \quad (13)$$

Using the inter-story displacements of the 2nd and 3rd stories, the restoring forces in the upper stories and the tangent stiffnesses were determined directly from the hysteretic model (see Table 5 for modeling parameters). The rearranged incremental EOM (Eq. (13)) was solved using Eqs. (6)-(11). Note that in Eq. (6), the Δp^i term was taken as the right-hand side of Eq. (13). This

process was repeated for all subsequent time steps till the end of the RTHS. It should be noted that Eq. (13) is an implicit equation and for a nonlinear system, iteration is required to solve the EOM. However, for a linear system, iteration is not required when solving for an implicit equation. To avoid iteration and to keep the error within a tolerable level, a very small time step was selected in this study (0.0025s). In other words, the incremental EOM was assumed linear within an integration time step.

3. RTHS controller development

Prior to the real-time controller development, a slow PSD hybrid simulation controller was developed and applied in a full-scale hybrid simulation of a two-story wood shear wall frame conducted at the University of Alabama (Griffith *et al.* 2013). Employing double trigger functions, the controller for the slow hybrid simulation adopted a step/hold loading pattern during the controller development at Western Michigan University (WMU) and a ramp/hold pattern at University of Alabama (UA) for the full-scale test. The experiences gained through the development of the slow hybrid simulation controller were used in the RTHS controller development focusing on the suitability for multiple testing facilities, experimental specimens of various scales and rapid deployment. Each development phase consisted of multiple experiments with controllers varied slightly from the previous to examine the effect of several strategies of improving accuracy and stability. Table 1 summarizes the milestone experiments in the controller development phase. “Open” type tests represent *open-loop simulation* during which loading histories (i.e., simulated structural displacement response) are predetermined as opposed to the general RTHS closed-loop test discussed in Section 1.

3.1 Benchmark scale pseudodynamic hybrid simulation at WMU

The RTHS controller development was initiated at the Laboratory for Earthquake and Structural Simulation (LESS) at WMU. LESS is equipped with a benchmark-scale hybrid testing system (Shao and Enyart 2012). A small-scale steel cantilever column was designed and fabricated specifically for the controller development purposes and was used as the test specimen, featuring easy replacement and predictable response. The test specimen and a schematic diagram of the hybrid simulation are shown in Fig. 3. A simulation model was created in the *hybrid simulation controller* using Matlab/Simulink which consisted of the numerical model of the test structure, the integration algorithm for solving the EOM (discussed in Section 2) and the compensator for inherent actuator delay and command tracking errors. The simulation model was then downloaded (deployed) to the *real-time controller* that would be running the simulation model in real time during a hybrid simulation and communicating with the *hydraulic controller*. The hydraulic controller received the step-by-step simulated target displacement commands from the real-time controller and drove the actuator to impose this displacement to the physical specimen. Meanwhile, the actuator load transducer measured the corresponding restoring force through the hydraulic controller onboard data acquisition system and fed this force back to the simulation model in the real-time controller to determine the next step displacement command.

Table 1 Milestone experiments in RTHS controller development

Lab	Type	Objective
WMU	Open	Determine optimum real-time controller operating rate; Estimate the time delay value of the WMU actuator
	Close	Choose between two time delay compensators using performance index; Optimize the estimated time delay value used in the compensator
UA	Open	Estimate time delay values of the UA high-speed large stroke actuator for two test specimens
	Close	Implement the RTHS controller and conduct full-scale experiments

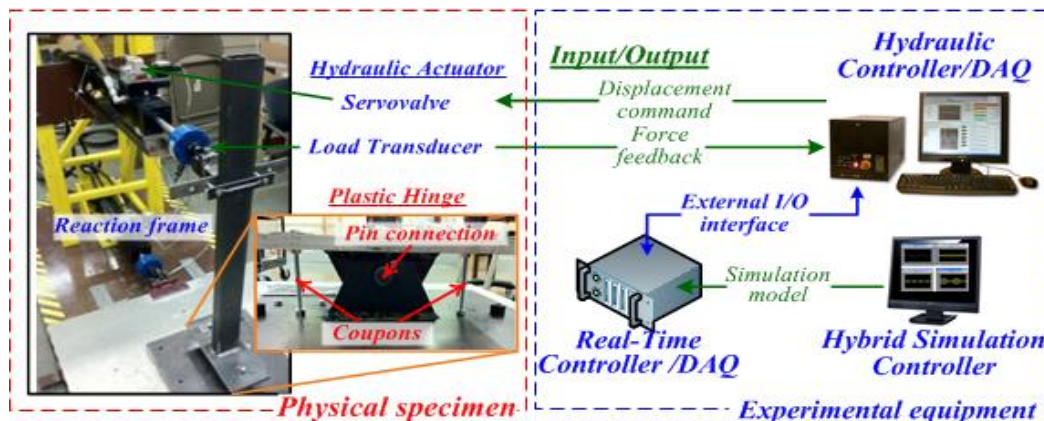


Fig. 3 Small-scale WMU specimen and LESS hybrid testing system

3.1.1 Open-loop development

Open-loop tests were conducted first with the objectives of tuning the actuator to its best command tracking performance and identifying the corresponding controller parameters. The PID gains in the hydraulic controller (i.e., SC6000 controller from ShoreWestern[®]) were adjusted using a square-wave cyclic excitation to obtain optimum actuator response. Then the open-loop tests were further carried out utilizing the real-time and the hybrid simulation controllers that would be used in the closed-loop RTHS. Thus calibration settings (i.e., conversion of voltage readings to engineering units of actuator force/displacement feedback and command) in the real-time controller can be validated. In addition, the optimum real-time controller operating rate was determined in this open-loop phase. The input displacement history to the actuator was the simulated seismic response of the first story using the 3DOF numerical model that would be used later in the full-scale RTHS. Two performance indices commonly used to evaluate the RTHS controller performance were used, namely the normalized peak error (NPE) and the root mean square (RMS) of the tracking error over the time history, which are defined as

$$NPE = \frac{\max(|d_i^d - d_i^m|)}{\max(|d_i^d|)} \times 100\% \tag{14}$$

$$RMS = \sqrt{\left(\frac{1}{N} \sum_{i=1}^N [d_i^d - d_i^m]^2\right) / \left(\frac{1}{N} \sum_{i=1}^N [d_i^d]^2\right)} \times 100\% \tag{15}$$

where N is the number of time steps, d_i^d is the desired displacement and d_i^m is the measured displacement. As shown in Table 2, the higher controller rate (i.e., 4000 Hz) provided better actuator performance in terms of smaller tracking errors and less time delay. Therefore, the 4000 Hz controller rate was adopted in the closed-loop development as discussed below.

3.1.2 Closed-loop development

The time delay in an actuator response must be compensated in a closed-loop RTHS to ensure stability and accuracy. Various compensation methods were developed in recent years at different laboratories specifically for their respective equipment and test specimen. In this project, the RTHS controller development was focused on easy implementation and rapid deployment at the WMU and UA laboratories with drastically different test specimens and equipment (see Table 4 for equipment comparison). Therefore a simple feed-forward based compensation algorithm was adopted and the parameters were optimized using the aforementioned performance indices. Both first-order and second-order feed-forward compensators, referred as FF and MFF, were tested as shown below (Lamarche *et al.* 2010, Dion *et al.* 2011)

$$\text{FF: } u_c^i = u_p(i\Delta t + \tau) = (1 + \eta)u^i - \eta u^{i-1} \tag{16}$$

$$\text{MFF: } u_c^i = u_p(i\Delta t + \tau) = \left(1 + \eta + \frac{\eta^2}{2}\right)u^i - \left(\eta + \frac{\eta^2}{2}\right)u^{i-1} + \left(\frac{\eta^2}{2}\right)u^{i-2} \tag{17}$$

in which i is the time index of the current integration step; Δt is the integration time step (same as the real-time controller time step in this RTHS); τ is the time delay estimated from open-loop tests and $\eta = \tau/\Delta t$ is a dimensionless control parameter. u_c^i is the command displacement at time step i which predicted the desired actuator's position u_p at the time instant of $i\Delta t + \tau$ based on the actuator's desired position of current step u^i and previous step(s). Thus by inputting the compensated command u_c^i to the actuator that considered the time delay effect, the resulting actuator's displacement became very close to the desired position u^i .

Table 2 Open-loop tests results

Real-time controller rate (Hz)	RMS(%)	NPE (%)	Time delay (sec)
1000	4.78	5.41	0.013
4000	3.91	3.68	0.010

Table 3 Evaluation of time delay compensators and optimizing τ

Compensator	Feed-forward (FF)		Modified Feed-forward (MFF)		
	τ (sec)	RMS(%)	NPE (%)	RMS(%)	NPE (%)
	0.10	3.93	4.55	3.51	4.15
	0.12	3.50	4.18	3.36	4.05
	0.014	4.13	4.42	3.74	4.23

These two compensator algorithms were implemented and their performance was compared at different estimated delay values τ and sample results are provided in Table 3. The sampling rate of the real-time controller was set to 4000 Hz throughout the closed-loop tests and the same 3DOF numerical model was employed with proper scaling to avoid damage to the test specimen so that repeated tests could be performed. As shown in Table 3, the MFF compensator provided consistently better performance than the FF compensator using the same estimated τ values. Also the least error indices were obtained when $\tau=0.012$ sec for both FF and MFF compensators, which is slightly larger than the actuator delay value estimated from open-loop tests (i.e., $\tau = 0.01$ sec). This may be attributed to the additional time delay introduced by the numerical simulation of closed-loop tests. Fig. 4 compares the displacement responses of two compensators using three τ values with the desired displacement and Fig. 5 compares their errors (i.e., the difference between the desired displacement and the measured displacements employing the compensators). A preliminary assessment of the data in Figs. 4 and 5 indicated that both MFF and FF compensators provided effective time delay compensation as the measured responses are reasonably close to the desired displacement histories and the peak errors are generally less than 0.02 inches. Through the close-up view of two peaks in Fig. 4 and comparing the error amplitudes in Fig. 5, it was concluded that the MFF compensator with $\tau=0.012$ sec provided the best time delay compensation performance for the WMU actuator and the test specimen, which is consistent with the conclusion made on the error index values shown in Table 3.

3.2 Large-scale controller implementation at UA

To implement the RTHS controller developed at WMU in the newly constructed Structural Engineering Laboratory at UA, a complete study on the UA equipment was conducted first focusing on identifying functional hybrid simulation controller components and characterizing hydraulic loading equipment. As shown in Table 4, both facilities use Matlab/Simulink to set up the simulation model allowing a fast migration of the WMU controller model to UA. Other controller components such as real-time controller, hydraulic controller and input/output (I/O) interfaces between these two controllers are similar at both sites.

However, the capacities (i.e., force capacity, stroke limit and maximum velocity) of the UA actuator are much greater as compared to the WMU counterpart. Therefore, to characterize the UA actuator performance (mainly the time delay and amplitude tracking error), several open-loop tests using different displacement command histories were conducted first. It was determined that the average RMS error of four open-loop tests was 1.695% (vs. the minimum RMS of 3.91% for the WMU tests), demonstrating that the UA hydraulic controller had a much better command tracking

performance. Open-loop tests of the two test specimens (i.e., shear wall specimen with and without damper installed) were conducted prior to the closed-loop RTHS to estimate the time delay values (for the two specimens, the estimated values were 0.005 and 0.008 sec, respectively). These two estimated delay values were then used in the MFF compensator for the RTHS.

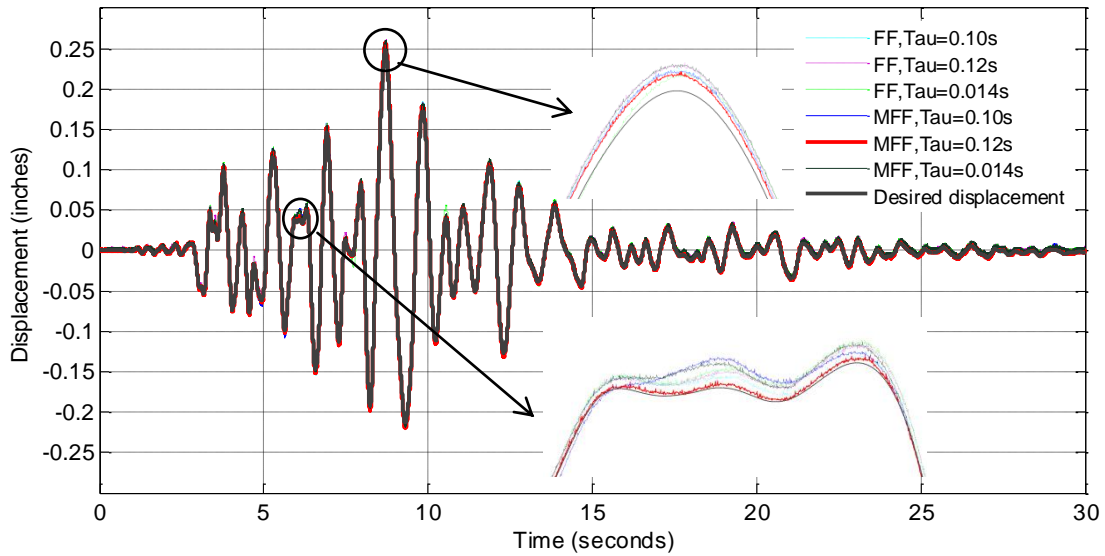


Fig. 4 Displacement responses of two compensators with varying τ

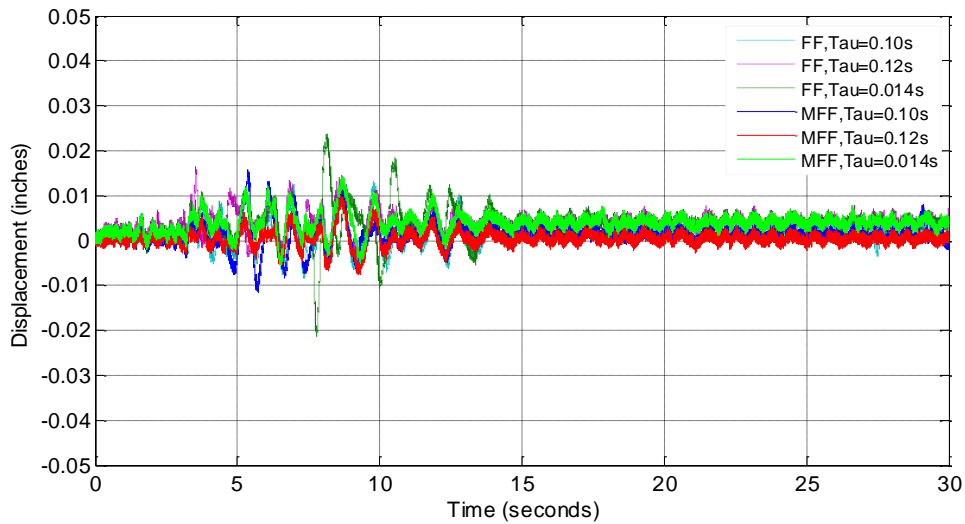


Fig. 5 Displacement errors of two compensators with varying τ

Table 4 Hybrid simulation testing system at WMU and UA

RTHS system components		WMU	UA
Hydraulic equipment	Model:	Shore Western 910D	MTS 244.31
	Linear hydraulic actuator	Force: ± 3.2 kips (13.3 kN)	± 55 kips
	Stroke:	± 3 inches (76.2 mm)	± 20 inches
	Max. velocity:	36 in/s (914.4 mm/s)	50 in/s (1,270 mm/s)
	Load transducer	2.5 kips (11.12 kN)	55 kips (245 kN)
Servo valve	10 gpm at 1000 psi	250 gpm at 2800 psi	
Controller components	Hydraulic controller	SW SC6000w/DAQ and user interface, operated at 4000 Hz	MTS Series 793 w/DAQ and testing software, operated at 1024 Hz
	Hybrid testing controller simulation software	Matlab/Simulink	Matlab/Simulink
	Hybrid testing controller interface to real-time controller	NI-VeriStand	Matlab/xPC Target
	External I/O interface	SCB-68 Connector Block	SCRAMNet GT150
	Real-time controller	NI 2.53 GHz Dual-Core PXI 8108 Controller	3.0 GHz Xeon Dual-Core Real-time Target PC

4. RTHS of multi-story wood shear wall equipped with rate-dependent energy dissipation device

The numerical simulation and the RTHS controller developed at Clemson and WMU respectively were subsequently implemented at UA via full-scale RTHS of a three-story stacked wood shear wall. Two first-story wall specimens were constructed and tested, one with a rate-dependent energy dissipation device (linear viscous damper) and the other without the device so that the RTHS results can be utilized to evaluate the effectiveness of the device on the seismic performance of the stacked wood shear wall.

4.1 Test structure and setup

The experimental substructure (i.e., the woodframe wall specimen representing the first story) was 20 ft (6.1 m) long, 8 ft (2.44 m) high and constructed using 2×6 nominal dimension lumber. The wall without the damper consisted of three full shear wall sections, with a window opening and a door opening. In all tests, 2×6 spruce-pine-fir (SPF) was used for studs and 15/32 in. (1.2 cm) plywood was installed for sheathing. Studs were placed at 16 in. (40.6 cm) on center and sheathing to framing nails (8d box nails) were installed at 6 in. (150 mm) on the panel perimeter and 12 in.

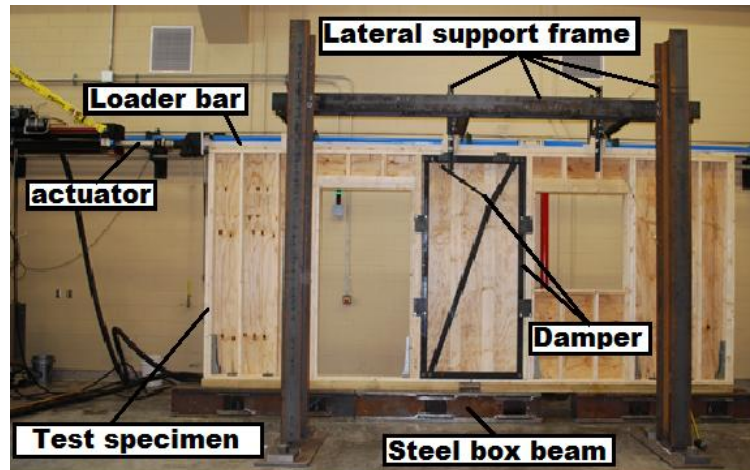


Fig. 7 Wood shear wall specimen and hybrid simulation setup

4.2 Cyclic test results and numerical substructure model calibration

The hysteretic behavior of the numerically-defined upper two stories was characterized through a quasi-static cyclic test of a full-scale wall specimen that had the same configuration as the test specimen shown in Fig. 6(a). The wall configurations are nominally identical for the second and third stories; hence, only one cyclic test was performed to characterize the hysteretic behavior of the numerical substructure. The CUREE loading protocol (Fig. 8(a)) was used (Krawinkler *et al.* 2001), which consists of three types of cycles, namely, *initiation*, *primary* and *trailing* cycles. The initiation cycles are very low amplitude cycles and are executed at the beginning of the loading history for checking the force-deformation response of the test equipment. The initiation cycles are followed by a series of primary and trailing cycles. A primary cycle is always followed by two or three trailing cycles that are 75% of the amplitude of the preceding primary cycle. The trailing cycles are used to capture the in-cycle stiffness and strength degradations. The amplitude of each primary cycle is larger than the preceding primary cycle and the actual amplitude is defined as a percentage of a reference displacement. A reference displacement of 3 in. (76.2 mm) was used in this test. The loading protocol and the resulting hysteretic response, along with a numerical fit of the data using the MSTEW hysteretic model, are shown in Fig. 8(b).

As can be seen in Fig. 8, the maximum displacement of the cyclic test was approximately 7.5 in. (160 mm), applied over a 175 sec time span. The initial stiffness of the test wall was determined to be 8.82 kips/in (1545 kN/m) with a displacement at peak force (δ) of 3.81 in. (96.8 mm) and a peak force (F_u) of 6.7 kips (29.8 kN). The results of the cyclic test were used to calibrate the parameters in the hysteretic model of the wall specimen; the resulting parameter values are given in Table 5. This model was used in the RTHS to determine the response of the numerical substructure (i.e., the response of the upper two stories).

Table 5 Values of parameters defining the hysteretic model for the second and third stories

K_o (kip/in)	r_1	r_2	r_3	r_4	F_o (kip)	F_i (kip)	δ (in)	α	β
8.82	0.067	-0.132	1.164	0.012	5.0	0.58	3.81	0.75	1.10

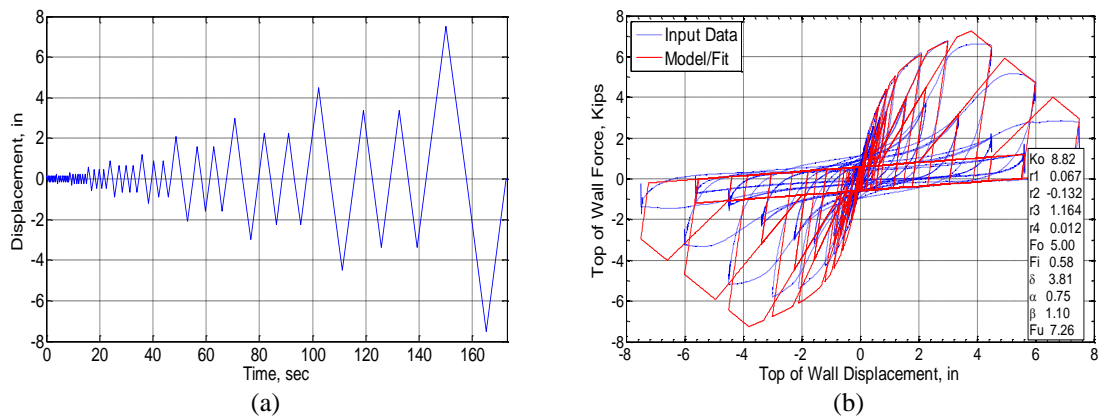


Fig. 8 Cyclic test (a) CUREE cyclic loading protocol and (b) test versus model hysteretic response for upper stories (1 in. = 0.0254 m, 1 kip = 4.448 kN)

4.3 Energy dissipation system

A linear viscous damper with damping coefficient of 0.26 kip-sec/in (45.55 kN-sec/m) was installed in a toggle-braced framing assembly (see Fig. 9(a)). The geometry of the toggle-braced framing results in an average displacement amplification factor of $f = 1.58$ over a displacement range of ± 1 in. (± 2.54 cm). The lateral resisting force that the toggle-braced damper provides is given by (Sigaher and Constantinou 2003)

$$F = C_o f^2 \dot{u} \tag{18}$$

where C_o is the damping coefficient and \dot{u} is the inter-story velocity. Note from Eq. (18) that the effective damping coefficient is proportional to the square of the average displacement amplification factor.

The damper, when installed within the toggle-braced frame, has a displacement capacity of 4.04 in. (102.6 mm) in extension and 2.02 in. (51.3 mm) in compression. With the bottom of the frame fixed in place, this would correspond to lateral displacement of the top of the frame to the left and right, respectively, as shown in Fig. 9(a). Furthermore, the axial force capacity of the damper is 4 kips (17.8 kN). Unlike other commonly used framing assemblies, the displacement amplification factor provided by the toggle assembly is highly nonlinear with larger amplification occurring when the damper is extended (damper extension corresponds to negative inter-story displacement in Fig. 9(b)). The nonlinearity in the displacement amplification factor was considered in the numerical simulation results presented in Section 5.2.

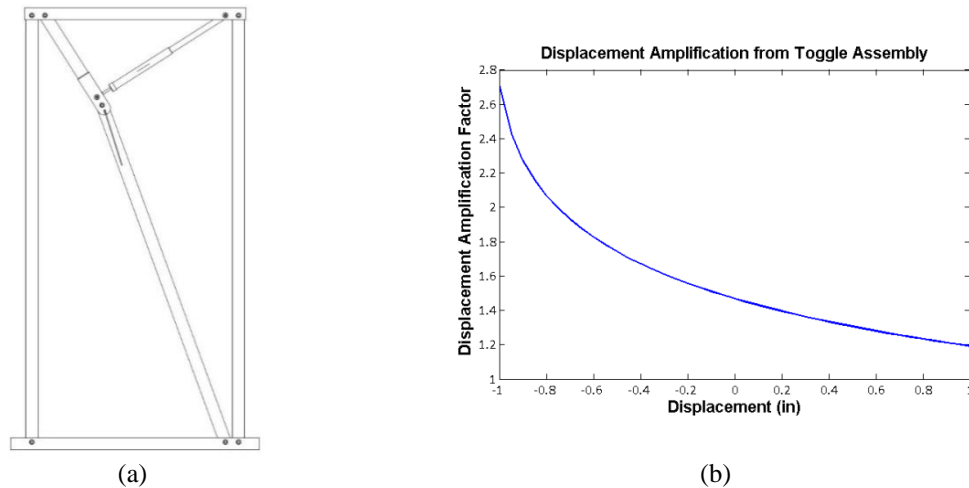


Fig. 9 Toggle-braced damper assembly: (a) geometry and (b) displacement amplification factor

4.4 RTHS program

The RTHS program for the three-story stacked wood shear wall with an experimental first story substructure consisted of two phases: 1) with viscous damper installed and 2) without viscous damper installed. Each phase consisted of two or three closed-loop experiments with increasing earthquake intensities as shown in Table 6. The earthquakes were selected based on the results of pre-test time-history analyses on the 3-DOF model with a fluid viscous damper in the first story. The 22 bi-axial FEMA P-695 far-field earthquakes (APC 2009) scaled to 30% Design Basis Earthquake (30%DBE), Design Basis Earthquake (DBE) and Maximum Considered Earthquake (MCE) levels for Southern California were utilized for the time-history analyses. The DBE and MCE levels correspond to earthquakes having 10% and 2% probabilities of exceedance in 50 years. Note that for each hazard level, 44 non-linear time history analyses were performed (22 ground motions \times 2 components). The maximum inter-story drift for each analysis was recorded and used to plot the cumulative distribution function (CDF) of the peak inter-story drifts for each of the three hazard levels considered (see Fig. 10). One of the ground motions recorded in California, the Northridge 1994 recorded at Beverly Hills (PEER ground motion ID: MUL009), was selected for this RTHS. This ground motion was selected because the predicted peak drifts for all three hazard levels were within the operational range of the damper. The test earthquake record scaled to 30%DBE, DBE and MCE levels are shown in Fig. 10 as filled-in circular markers. The recorded peak ground acceleration (PGA) and magnitude of this earthquake were 0.52 g and 6.7 g, respectively. The scaled PGA for RTHS are listed in Table 6.

It is worth noting that the second phase RTHS was conducted two months later than the first phase and with three participants collaborating using the Team Viewer remote PC control program. The hybrid testing controller PC at UA was remotely controlled from WMU to compile the simulation model and download to the xPCTarget for real-time execution. The numerical model parameters and earthquake input were verified by researchers at Clemson University before each RTHS through remote access of the Matlab initialization script. In addition, the MTS hydraulic

equipment was operated by a local UA investigator to ensure the safety of lab users and for protection of both the equipment and the test specimen.

5. RTHS results and discussion

5.1 Time history response

The time-delay compensator was successfully implemented during the RTHS and their performance indices (defined in Section 3.1.1) are provided in Table 7. Both the integration step and the real-time controller step were 1/1024 sec for all the UA RTHS tests. As an example, Fig. 11 shows the comparison of the desired displacement and the measured displacement for Test b (Shao *et al.* 2014). The displacements match very well and thus the RTHS controller is considered to be acceptable (i.e., the RTHS results are deemed reliable for the purpose of seismic response assessment).

Table 6 Summary of RTHS experiments

	ID	Acceleration inputlevel	PGA (CU)	Specimen
Phase 1	a	30% DBE	0.1064 g	Damped wall
	b	100% DBE	0.3548 g	
Phase 2 (remote testing)	c	30% DBE	0.1064 g	Undamped wall
	d	100% DBE	0.3548 g	
	e	100% MCE	0.5322 g	

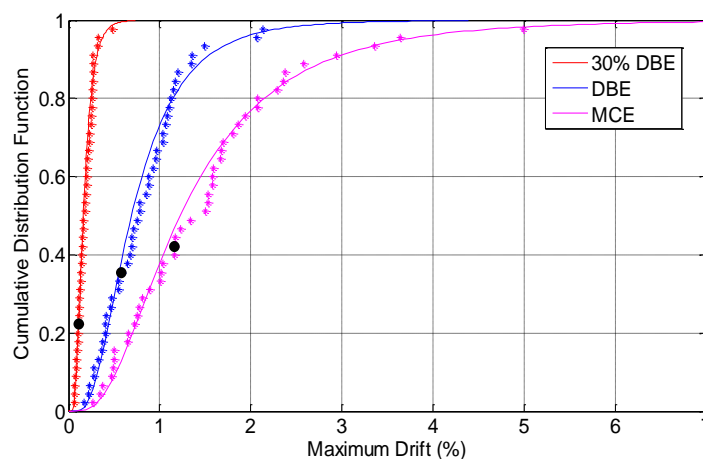


Fig. 10 Peak inter-story drift distributions for 30%DBE, DBE, and MCE levels determined using a pre-test numerical model for the 3-story wall system with damper

Table 7 Performance index values for RTHS controller

Test ID	Specimen	τ (sec)	RMS (%)	NPE(%)
a	Damped wall	0.005	1.53	3.03
b			2.13	2.64
c	Undamped wall	0.008	4.09	4.26
d			4.42	5.29
e			1.77	3.54

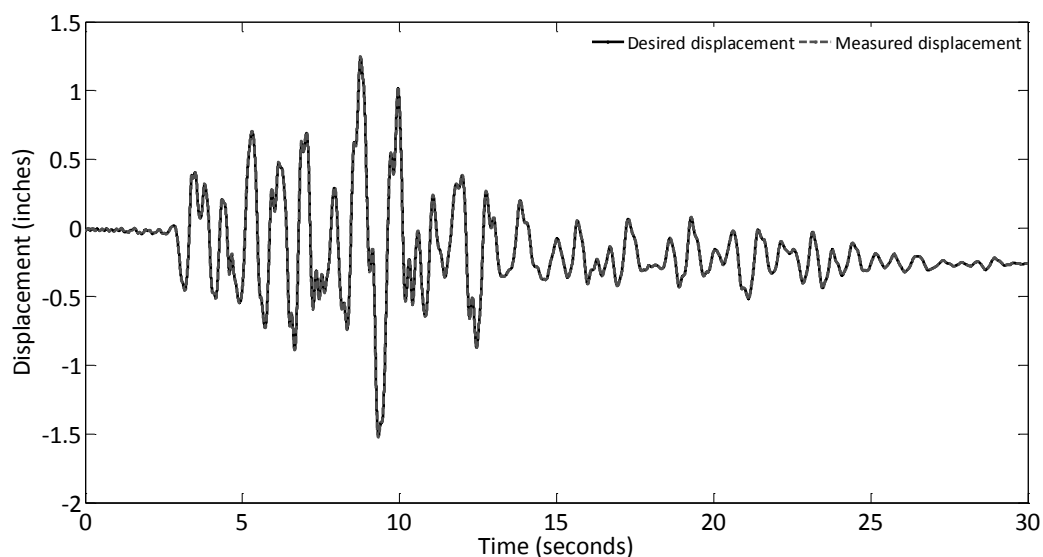


Fig. 11 Comparison of desired and measured time-history response of damped wall at 100% DBE excitation

5.2 Hysteretic responses

The experimental response and numerically-predicted response of the first story physical substructure with and without damper installed during Tests b and d (structure subjected to 100% DBE level excitation) are shown in Fig. 12 (Shao *et al.* 2014). Reasonable agreement is achieved between the numerical and experimental hysteretic loops for the damper wall test. For the wall without damper, the discrepancy between the numerical model and experimental results are apparent. This discrepancy is likely due to the difference in boundary conditions between the model and the physical substructure shear wall. The numerical model assumes pure in-plane behavior of the wall. During the RTHS, roller supports between the loader bar and lateral support frame along the top of wall were provided to brace the test specimen against out-of-plane movement (see Fig. 7), as assumed in the numerical model. However, some out-of-plane vibration was observed, which could have caused the difference between the test and model results.

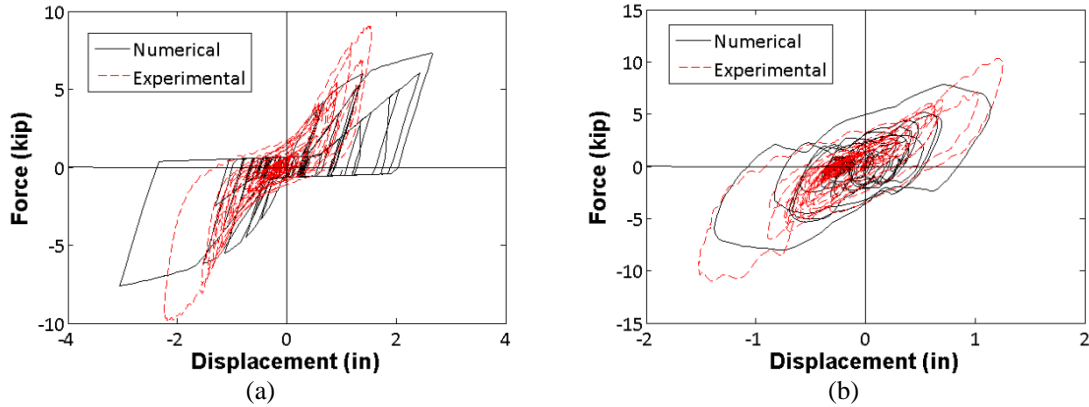


Fig. 12 Comparison of numerical and experimental hysteretic response of physical substructure: (a) without damper and (b) with damper

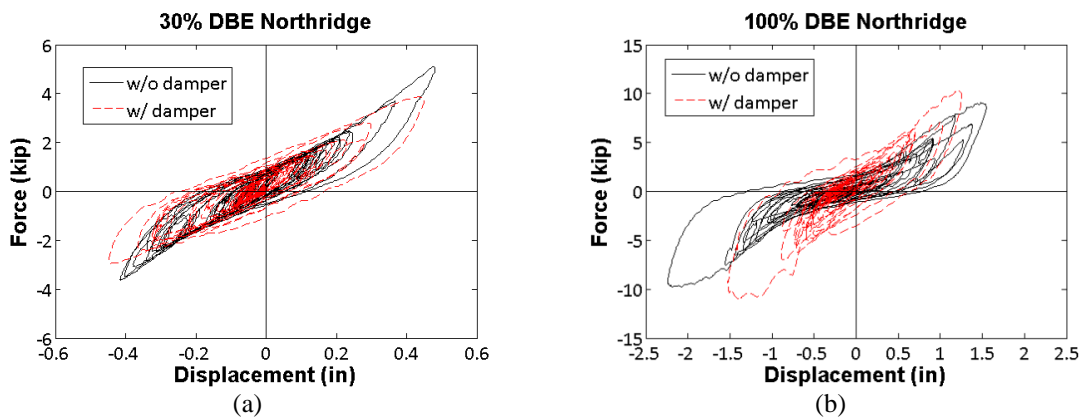


Fig. 13 Comparison of experimental shear wall response for physical substructure: (a) 30% DBE excitation and (b) 100% DBE excitation

Although wood shear walls generally exhibit higher variability in hysteresis shape and resulting parametric fits, this typically would result in moderate effect on the hybrid simulation of moderate responses that do not reach the peak capacity (i.e., do not move to the descending branch of the hysteretic model). However, it should be noted that when there is a large discrepancy between the numerical and experimental hysteretic response (as shown in Fig. 12 (a) for the undamped wood shear wall specimen after 1" displacement), whether caused by epistemic or aleatoric uncertainties, this would result in reduced accuracy in the RTHS results. The effects of such discrepancy in RTHS results can be assessed using a reliability approach proposed by Chen *et al.* (2013) at different hazard levels, which is beyond the scope of this paper. In the subsequent full-scale three-story hybrid simulation carried out at the NEES facility at the University at Buffalo, the parameters of the numerical model were selected to closely reproduce the prototype structural response and great care was taken in the design and construction of the experimental substructure,

especially the boundary conditions, to improve the reliability of hybrid simulation results (Pang *et al.* 2014).

A direct comparison of the hysteretic response of the wall specimen with and without the damper is shown in Fig. 13 (Shao *et al.* 2014). It is observed that the damper assembly improves the performance of the wood shear wall by providing a supplemental energy dissipation mechanism and thus reducing the energy dissipation demand on the shear wall framing system (i.e., reducing nonlinear hysteretic response in the wood framing system). This nonlinear deformation is directly associated with structural damage. Focusing on the 100% DBE level excitation, Fig. 13(b) shows that: (1) The damper reduces the maximum displacement (inter-story drift) of the wall by 32%; (2) The strongly pinched shape of the hysteresis loops for the wall without damper is virtually eliminated for the case of the shear wall protected with the damper (due to ability of the viscous damper to dissipate large amounts of energy in the small displacement region of the response); and (3) The peak force for the shear wall retrofitted with a damper is increased by a relatively small amount (13.8%) compared to that of the wall without the damper. These observations are of particular interest to the NEES-Soft project where much attention is given to retrofitting the soft ground story while avoiding any significant transfer of damage to the upper stories. The RTHS results clearly suggest that a retrofit that focuses on energy dissipation may be advantageous over stiffness-based retrofits since the maximum inter-story drifts can be reduced without a significant increase in forces.

In spite of the potential of supplemental damping to improve the seismic performance of light-framed wood structures, as demonstrated in the RTHS testing, successful application remains a challenge due to a number of factors (e.g., the inherent flexibility of wood framing connections leads to losses in displacement transfer between the wood framing system and the damper assemblies). Since the damper displacement and the toggle frame deformation were not directly measured, the losses in displacement transfer could not be experimentally determined. However an estimate of the losses can be obtained by using the results from numerical simulations. For the case of 100% DBE excitation, a maximum displacement of 1.37 in. (34.8 mm) was calculated while the corresponding measured displacement from the RTHS tests was 1.52 in. (38.6 mm) (see Fig. 13(b)). The increased displacement in the experimental results (about 11% increase) may be attributed, at least in part, to the loss of displacement transfer from the wood framing to the toggle-braced damper. It may be concluded that, from a displacement transfer perspective, the toggle-braced damper performed reasonably well in the RTHS, having a displacement transmission efficiency of about 89%. The effectiveness of the toggle-braced damper configuration will be further investigated using the results from the shaking table tests of a four-story soft-story building that was tested as part of the NEES-Soft project (Tian *et al.* 2014 and van de Lindt *et al.* 2014).

5.3 Wood shear wall damage

The shear wall without damper was tested with ground motion recorded during the 1994 Northridge, CA earthquake and scaled with different intensities: 30% and 100% DBE. The damage observed after the 30% DBE ground motion (Test c in Table 6) was negligible. There were a few sheathing edge nails that were withdrawn by a small amount of less than 1/8 in. (3.2 mm) while the rest of the sheathing nails were intact (see Fig. 14(a)). The observed damage was consistent with data obtained from the hysteretic curves shown in Fig. 13a. With a maximum lateral displacement of about 0.45 in. (11.43 mm), the behavior of the shear wall was still in the elastic

range. The ground motion intensity was then scaled up to 100% DBE (Test d), resulting in damage that was readily observed. The sheathing edge nails of the sheathing panel on the left and the middle panel were withdrawn by about 0.5 to 1.5 in (12.7 to 38.1 mm) (see Figs. 14(b) and 14(c)). The number of withdrawn nails also increased significantly, which is consistent with the hysteretic data obtained and shown in Fig. 13(b). With a maximum lateral displacement of 2.25 in. (57.1 mm) for the 100% DBE case, the behavior of the shear wall was clearly in the inelastic range. Due to the failure of the sheathing edge nails, the shear capacity of the entire wall also decreased significantly.

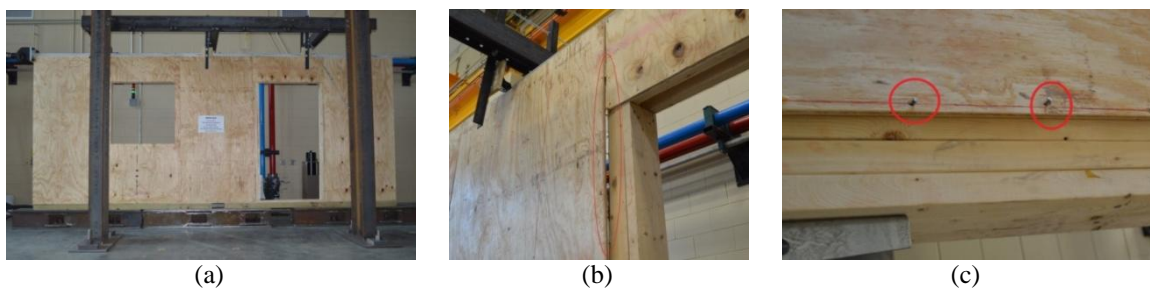


Fig. 14 Damage observed from RTHS tests of the shear wall without damper (a) 30% DBE, (b) 100% DBE (Panel edge opening) and (c) 100% DBE (Panel edge nail pulled-out)

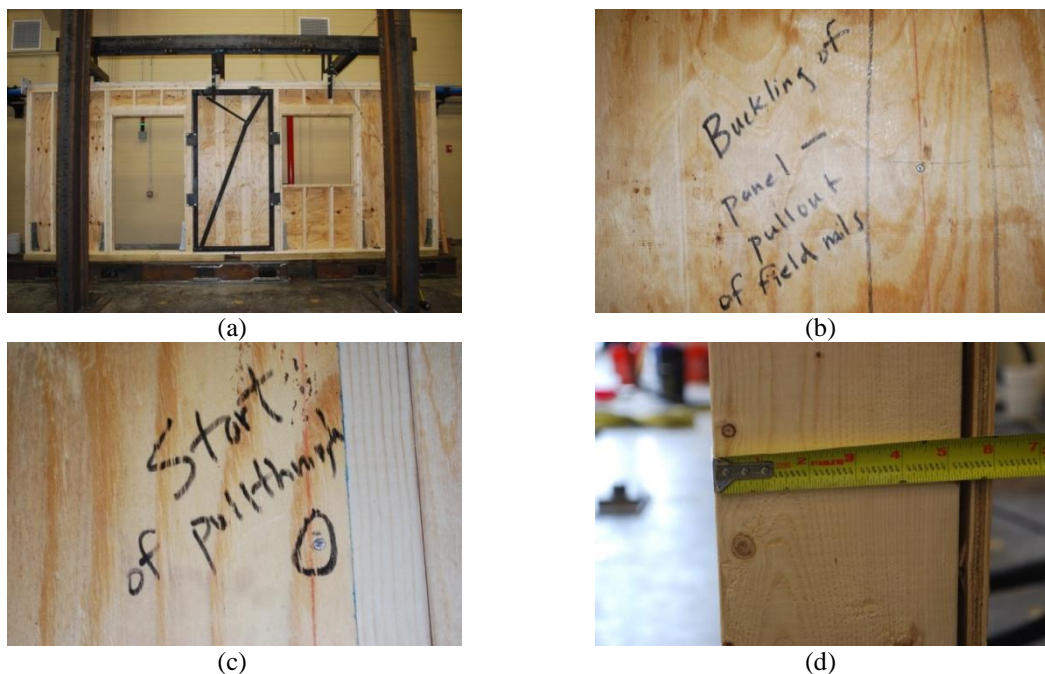


Fig. 15 Damage observed from RTHS tests of the shear wall with damper (a) Damped wall after 30% DBE test; (b) Field nail pulled out after 100%DBE test; (c) Edge nail pull-through and (d) Edge nail pull-out

The shear wall with damper was tested using the same earthquake ground motion scaled at 30% and 100% DBE. After the 30% DBE test (Test a), no damage was observed in the wall (see Fig. 15(a)). The maximum displacement during the 30% DBE test (see Fig. 13(a)) also indicated that the wall was still in the elastic range and self-centered after the test. At this loading level, the inter-story velocity was small and thus the effect of the damper was not clearly observed. The wall was then subjected to the 100% DBE ground motion (Test b) with the expectation that the influence of the damper on the performance of the wall would become evident. At this excitation level, the damage pattern was similar to what was observed at the same excitation level for the wall without damper, but was at a reduced severity. Due to buckling of the sheathing panels (in the center panel), some of the sheathing field nails exhibited slight pulled-out (see Fig. 15(b)). In addition, some of the sheathing edge nails showed a pulled-through failure while others exhibited a pulled-out failure with about 0.25 in. (6.34 mm) protrusion (see Figs. 15(c) and 15(d)).

6. Conclusions

Large-scale real-time hybrid simulations (RTHS) of wood shear wall systems were conducted at the Structural Engineering Laboratory at The University of Alabama (UA). In order to develop the RTHS controller, a series of benchmark-scale RTHS tests of a steel cantilever column specimen were carried out at Western Michigan University (WMU) to optimize controller settings and compensator parameters. This controller features a simple algorithm and easy adaptation to new testing equipment leading to a fast migration to the UA laboratory for the large-scale RTHS with minimum development effort. It was demonstrated from RTHS results (from both benchmark-scale and large-scale experiments) that the developed RTHS controller successfully compensated for the actuator time delay and provided reliable experimental data.

The developed controller was subsequently applied to the full-scale RTHS of two three-story wood shear wall systems to subject the experimental substructure to realistic seismic loading as if it were part of a complete structural system. The experimental substructures were the first-story shear wall with and without a rate-dependent damping device (viscous damper) and the numerical substructure was the upper two stories of the multi-story stacked shear walls. A modified Newmark- β integration algorithm was used to determine the simulated displacement response of the first story wall and was subsequently applied to the test wall via a hydraulic actuator. The hysteretic CASHEW model was used to model the response of the numerical upper two stories. The wood shear wall specimen exhibited realistic hysteretic behavior and realistic damage patterns, demonstrating that RTHS is a reliable experimental method to study the seismic response of wood-framed structures, particularly those that include rate-dependent seismic protection devices that require real-time testing. The control scheme developed in this set of experiments served as the basis for the development of the full-scale slow pseudodynamic hybrid simulation that were carried out simulation on a three-story wood-framed building at the NEES facility at the University at Buffalo.

The ability of the damper at the first level to effectively reduce the inter-story drift and damage to the wood shear wall was notable. Although there was only a slight reduction at the smaller more common seismic intensity of 30% DBE, the reductions were significant at a seismic intensity of 100% DBE. Specifically, a 32% reduction in the inter-story drift was observed and much less damage occurred (although some buckling of the sheathing panel was observed where the damper was located).

Acknowledgments

This work was primarily supported by the National Science Foundation under Award No. CMMI-104163 and 1314957. The authors would like to thank the Department of Civil, Construction and Environmental Engineering of the University of Alabama for providing access to the large-scale Structural Engineering Laboratory and for the assistance in wall construction.

References

- Ahmadizadeh, M. and Mosqueda, G. (2008), "Hybrid simulation with improved operator-splitting integration using experimental tangent stiffness matrix estimation", *J. Struct. Eng. - ASCE*, **134**(12), 1829-1838.
- Applied Technology Council (2009), *Quantification of Building Seismic Performance Factors*, FEMA P-695, Federal Emergency Management Agency, Washington, DC
- Carrion, J.E. and Spencer, B.F. (2008), "Real-time hybrid testing using model-based delay compensation", *Smart Struct. Syst.*, **4**(6), 809-828.
- Chae, Y., Ricles, J. and Sause, R. (2013), "Large-scale experimental studies of structural control algorithms for structures with magnetorheological dampers using real-time hybrid simulation", *J. Struct. Eng. - ASCE*, **139**, 1215-1226.
- Chen, C., Ricles, J.M., Marullo, T.M. and Mercan, O. (2008), "Real-time hybrid testing using the unconditionally stable explicit CR integration algorithm", *Earthq. Eng. Struct. D.*, **38**(1), 23-44.
- Chen, C., Sharma, R. and Pong, W. (2013), "Assessing reliability of real-time hybrid simulation results using a probabilistic approach", *Proceedings of the 15th World Conference on Earthquake Engineering*. Lisbon, Portugal.
- Darby, A.P., Blakeborough, A. and Williams, M.S. (1999), "Real-time substructure tests using hydraulic actuator", *J. Eng. Mech.- ASCE*, **125**(10), 1133-1139.
- Dion, C., Bouaanani, N., Tremblay, R., Lamarche, C.P. and Leclerc, M. (2011), "Real-time dynamic substructuring testing of viscous seismic protective devices for bridge structures", *Eng. Struct.*, **33**(12), 3351-3363.
- Dion, C., Bouaanani, N., Tremblay, R. and Lamarche, C. (2012), "Real-time dynamic substructuring testing of a bridge equipped with friction-based seismic isolators", *J. Bridge Eng.*, **17**(1), 4-14.
- Dolan, J.D. (1989), *The dynamic response of timber shear walls*, Ph.D.thesis, Univ. of British Columbia, Vancouver, Canada.
- Folz, B. and Filiatrault, A. (2001), "Cyclic analysis of wood shear walls", *J. Struct. Eng.- ASCE*, **127**(4), 433-441.
- Griffith, C., Shao, X., van de Lindt, J.W., Bahmani, P., Pang, W. and Ziaei, E. (2013), "Hybrid simulation of a wood shear wall frame", *Proceedings of the ASCE 2013 Structures Congress*, Pittsburgh, PA.
- Horiuchi, T., Inoue, M., Konno, T. and Namita, Y. (1999), "Real-time hybrid experimental system with actuator delay compensation and its application to a piping system with energy absorber", *Earthq. Eng. Struct. D.*, **28**(10), 1121-1141.
- <http://www.teamviewer.com/en/index.aspx>, last accessed June 30, 2013.
- Kamada, T., Yasumura, M., Yasui, S., Davenne, L. and Uesugi, M. (2011), "Pseudodynamic tests and earthquake response analysis of timber structures III: three-dimensional conventional wooden structures with plywood-sheathed shear walls", *J. Wood Sci.*, **57**(6), 484-492.
- Krawinkler, H., Parisi, F., Ibarra, L., Ayoub, A. and Medina, R. (2001), *Development of a testing protocol for woodframe structures*, CUREE Publication, No. W-02, Richmond, Calif.
- Lamarche, C.P., Tremblay, R., Léger, P., Leclerc, M. and Bursi, O.S. (2010), "Comparison between real-time dynamic substructuring and shake table testing techniques for nonlinear seismic applications",

- Earthq. Eng. Struct. D.*, **39**(12),1299-1320.
- Mercan, O. and Ricles J.M. (2009), "Experimental studies on real-time testing of structures with elastomeric dampers", *J. Struct. Eng.- ASCE*, **135**(9), 1124-1133.
- Nakashima, M. Kato, H. and Takaoka, E. (1992), "Development of real-time pseudo dynamic testing", *Earthq. Eng. Struct. D.*, **21**(1), 79-92.
- Pang, W., Rosowsky, D.V., Pei, S. and van de Lindt, J.W. (2007), "Evolutionary parameter hysteretic model for wood shearwalls", *J. Struct. Eng.- ASCE*, **133**(8), 1118-1129.
- Pang, W., Ziaei, E., Shao, X. and van de Lindt, J. (2014), "Collapse modeling and hybrid simulation of a three-story light-frame wood building", *Proceedings of the ASCE 2014 Structures Congress*, Boston, April, 3-5.
- Phillips, B. and Spencer, B., Jr. (2013), "Model-based feed forward-feedback actuator control for real-time hybrid simulation", *J. Struct. Eng. - ASCE*, **139**, 1205-1214.
- Richard, N., Yasumura, M. and Davenne, L. (2003), "Prediction of seismic behavior of wood-framed shear walls with openings by pseudodynamic test and FE model", *J. Wood Sci.*, **49**(2), 145-151.
- Saouma, V., Haussmann, G., Kang, D. and Ghannoum, W. (2013), "Real time hybrid simulation of a non-ductile reinforced concrete frame", *J. Struct. Eng.- ASCE*, 10.1061/(ASCE)ST.1943-541X.0000813 (Feb. 1, 2013).
- Shao, X. and Enyart, G. (2012), "Development of a versatile hybrid testing system for seismic experimentation", *Exp. Tech.*, 10.1111/j.1747-1567.2012.00837.x.
- Shao, X., van de Lindt, J.W., Bahmani, P., Pang, W., Ziaei, E., Symans, M., Tian, J. and Dao, T. (2014), *Real-Time Hybrid Simulation of Multi-story Wood Shear Walls*, Network for Earthquake Engineering Simulation (NEES)(distributor). Dataset. DOI: TBD.
- Shing, P.B., Stavridis, A., Wei, Z., Stauffer, E., Wallen, R. and Jung, R.Y. (2006). "Validation of a fast hybrid test system with substructure test", *Proceedings of the 17th Analysis and Computation Specialty Conference*, St. Louis, Missouri, USA.
- Sigaher, A.N. and Constantinou, M.C. (2003), "Scissor-jack-damper energy dissipation system", *J. Earthq. Spectra.*, **19**(1), 133-158.
- Stewart, W.G. (1987), *The seismic design of plywood sheathed shearwall*, Ph.D. Thesis, Univ. of Canterbury, Christchurch, New Zealand.
- Tian, J., Symans, M.D., Gershfeld, M., van de Lindt, J.W., Bahmani, P., Ziaei, E., Pang, W. and Shao, X. (2014), "Seismic performance of a full-scale soft-story woodframed building with energy dissipation retrofit", *Proceedings of the 10th National Conf. on Earthquake Engineering* (10NCEE), Anchorage, Alaska, July.
- van de Lindt, J.W., Symans, M.D., Pang, W., Shao, X. and Gershfeld, M. (2012), "The NEES-Soft project: Seismic risk reduction for soft-story woodframe buildings", *Proceedings of the 15th World Conference on Earthquake Engineering*, Lisbon, Portugal, September 24-28.
- van de Lindt, J., Bahmani, P., Pryor, S., Mochizuki G., Gershfeld, M., Pang, W., Ziaei, E., Jennings, E., Symans, M. Shao, X., Tian, J. and Rammer, D. (2014), "NEES-Soft experimental program for seismic risk reduction of soft-story woodframe buildings", *Proceedings of the ASCE 2014 Structures Congress*, Boston, April, 3-5.
- Yasumura, M. and Yasui, S. (2006), "Pseudodynamic tests and earthquake response analysis of timber structures I: plywood-sheathed conventional wooden walls with opening", *J. Wood Sci.*, **52**(1), 63-68.
- Yasumura, M., Kamada, T., Imura, Y., Uesugi, M. and Daudeville, L. (2006), "Pseudodynamic tests and earthquake response analysis of timber structures II: two-level conventional wooden structures with plywood sheathed shear walls", *J. Wood Sci.*, **52**(1), 69-74.